Available online at www.sciencedirect.com
ScienceDirect
Trans. Nonferrous Met. Soc. China 34(2024) 2743−2755
Transactions of Nonferrous Metals Society of China
www.tnmsc.cn

Damping properties and mechanism of aluminum matrix composites reinforced with glass cenospheres

Kai SUN[1], Lin WANG[1], Hang SU[2], Jia-yi GENG[1], Qiang ZHANG[1], Bo MENG[3], Zeng-yan WEI[1], Gao-hui WU[1]

1. School of Materials Science and Engineering, Harbin Institute of Technology, Harbin 150001, China;
2. State Key Laboratory for Performance and Structure Safety of Petroleum Tubular Goods and Equipment Materials, Xi'an 710000, China;
3. Shandong Quality Inspection and Testing Center of Construction Engineering, Shandong Academy of Building Research Co., Ltd., Jinan 250031, China

Received 24 February 2023; accepted 9 November 2023

Abstract: The damping properties were improved by preparing Al matrix composites reinforced with glass cenospheres through the pressure infiltration method. Transmission electron microscopy and scanning electron microscopy were employed to characterize the microstructure of the composites. The low-frequency damping properties were examined by using a dynamic mechanical thermal analyzer, aiming at exploring the changing trend of damping capacity with strain, temperature, and frequency. The findings demonstrated that the damping value rose as temperature and strain increased, with a maximum value of 0.15. Additionally, the damping value decreased when the frequency increased. Dislocation damping under strain and interfacial damping under temperature served as the two primary damping mechanisms. The increase in the density of dislocation strong pinning points following heat treatment reduced the damping value, which was attributed to the heat treatment enhancement of the interfacial bonding force of the composites.

Key words: glass cenospheres; Al matrix composites; microstructure; low-frequency damping properties

1 Introduction

Vibrations and noise are the most common issues in engineering applications currently [1,2]. The response and reconnaissance capabilities in the field of national defense are severely constrained by the noise and vibration of submarine gears. The noise produced by rocket engines and other components in manned space technology is detrimental to the physiological and psychological health of astronauts [3,4]. Thus, it is essential to develop materials that perform exceptionally well in dampening vibration and noise in addition to finding solutions to the vibration and noise problem. Polymers are the main focus of conventional shock and sound-absorbing materials [5,6]. The internal friction of the chain segments transforms the applied mechanical energy into thermal energy, serving as their damping mechanism. This phenomenon of motion hysteresis is caused by the unique molecular structure of polymer materials under the action of changing loads [7]. However, polymer materials are not as useful in other applications due to their low strength, poor heat resistance, and short service life.

In recent years, researchers have concentrated on the investigation of high-damping metal alloys [8−10]. However, high density and low specific strength are still drawbacks of high-damping

Corresponding author: Qiang ZHANG, Tel: +86-18246170339, E-mail: zhang_tsiang@hit.edu.cn;
Hang SU, Tel: +86-18845618587, E-mail: suhang12@cnpc.com.cn
DOI: 10.1016/S1003-6326(24)66573-8

alloys. Aluminum (Al) is characterized by lightweight. The damping values of Al alloy and Al matrix composites are $(1−2)\times10^{-3}$ and $(6−7)\times10^{-3}$, respectively [11,12]. These materials are not suitable for current vibration and noise-dampening applications that currently require damping values >0.1. Metal foam is a kind of lightweight material with various pore structures, which has attracted extensive attention in recent years and is often regarded as the best damping material [13−16]. BANHART et al [17] studied the damping performance of Al foam. Later, more researchers further studied the damping characteristics of Al matrix composites [18,19]. The research on Al matrix composites mainly focuses on using particles or short fibers as reinforcements. Considering the excellent damping performance of foam materials, it is necessary to further study the syntactic foam that directly applies hollow ceramic spheres as reinforcements.

Herein, a pressure infiltration method was employed to prepare glass cenospheres (GCs)/Al composites. To the best of our knowledge, a comprehensive analysis was first conducted on how the low-frequency damping performance of GCs/Al composite materials changed with increasing strain and temperature. The relationship among compressive strength of cenosphere, matrix alloys, and heat treatment techniques was also discussed in relation to the composites. The correlation between the storage modulus and loss modulus was analyzed. The damping value of Al matrix composites reached up to 0.15 in the presence of GCs, which was an order of magnitude higher than that of traditional Al alloys. Lower density of GCs/1100Al compared to that of Al alloys is good for noise reduction applications.

2 Experimental

2.1 Sample preparation

1100Al and AA6061 were provided by the Northeast Light Alloy Co., Ltd., China. The chemical composition of the matrix is listed in Table 1. The features of S38 and K46 GCs, which were acquired from 3M's Scotchlite product, are listed in Table 2. The shapes of K46 GCs are shown in Fig. 1, with spherical geometries and flawless surfaces.

GCs/Al composites were prepared through the pressure infiltration method. Firstly, broken GCs were filtered away using the flotation method and then dried at 60 °C for 12 h [20]. Next, GCs were placed in a steel mold. The volume fraction of GCs maintained at approximately 60%. The pressure infiltration mold and preform were heated to 800 and 600 °C, respectively. Subsequently, a 15 MPa

Table 1 Chemical composition of matrix (wt.%)

Matrix	Cu	Mg	Mn	Fe
1100Al	0.005	–	–	0.003
AA6061	0.43	0.75	0.22	0.36

Matrix	Si	Zn	Ti	Cr	Al
1100Al	0.0025	–	–	–	Bal.
AA6061	1.26	<0.15	<0.05	0.04	Bal.

Table 2 Physical properties of GCs

GC	Diameter/μm	ρ_{true}/(g·cm^{-3})	Porosity/%	Compressive strength/MPa
S38	40	0.38	85.04	27.56
K46	40	0.46	81.89	41.34

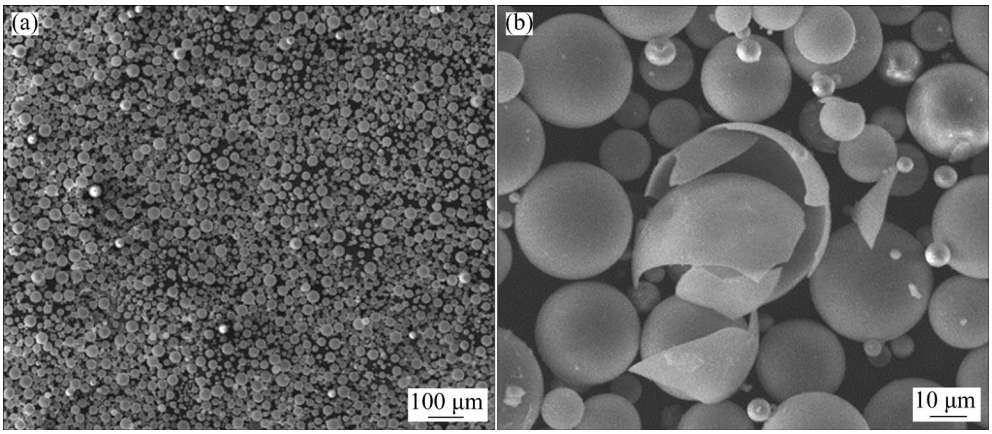

Fig. 1 SEM images of K46 GCs

pressure was added and maintained for 15 min while molten 1100Al and AA6061 were infiltrated. Al matrix composites were produced after cooling at a rate of 10 °C/min to room temperature.

2.2 Microstructure characterization and damping property measurement

Scanning electron microscopy (SEM) and transmission electron microscopy (TEM) images of samples were observed using an FEI Quanta 200FEG scanning electron microscope and a JEM−2010F transmission electron microscope, respectively. Quasi-static compression tests were performed using an Instron 5569 universal testing system with a cross-head speed of 1 mm/min. The damping capability was measured in the forced and bending vibration modes using a multifunctional internal friction apparatus (MFIFA). The damping strain spectrum test conditions were set as a test temperature of 25 °C, a strain amplitude range of 6×10^{-6}–3×10^{-3}, and a vibration frequency of 1 Hz. The test circumstances for the damping temperature spectrum were obtained with a strain amplitude of 1×10^{-3}, a test temperature range of 25−400 °C, and vibration frequencies of 0.5, 1, 10, and 20 Hz. To increase the statistical significance of the findings, at least five samples were used for each compressive and damping test in this work.

3 Results and discussion

3.1 Microstructures of GCs/Al composites

The microstructures of the GCs/Al composite materials are shown in Fig. 2. The matrix and the spherical area corresponded to the GCs, with uniform distribution. The majority of GCs remained in their original and intact structure, indicating that pressure infiltration did not cause the GCs to fracture.

Figure 3 displays the TEM images of the GCs/1100Al composites. The interface is comparatively smooth and flat in the absence of interfacial reactants, as shown in Fig. 3(a). The distribution of 1100Al in GCs/1100Al composites is shown in Fig. 3(b). No precipitate appeared, and numerous dislocations were derived from the thermal mismatch stress produced during the preparation procedure [21]. The interface between the GCs and

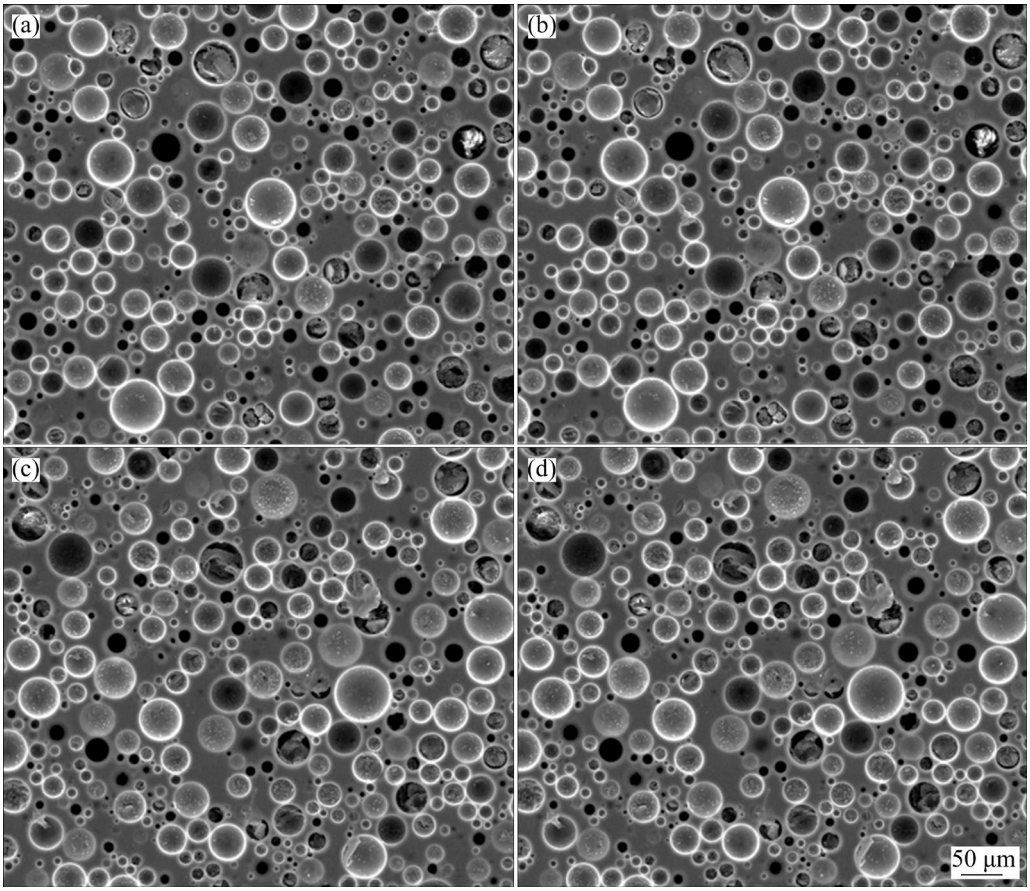

Fig. 2 Microstructures of GCs/Al composites: (a) S38/1100Al; (b) K46/1100Al; (c) S38/AA6061; (d) K46/AA6061

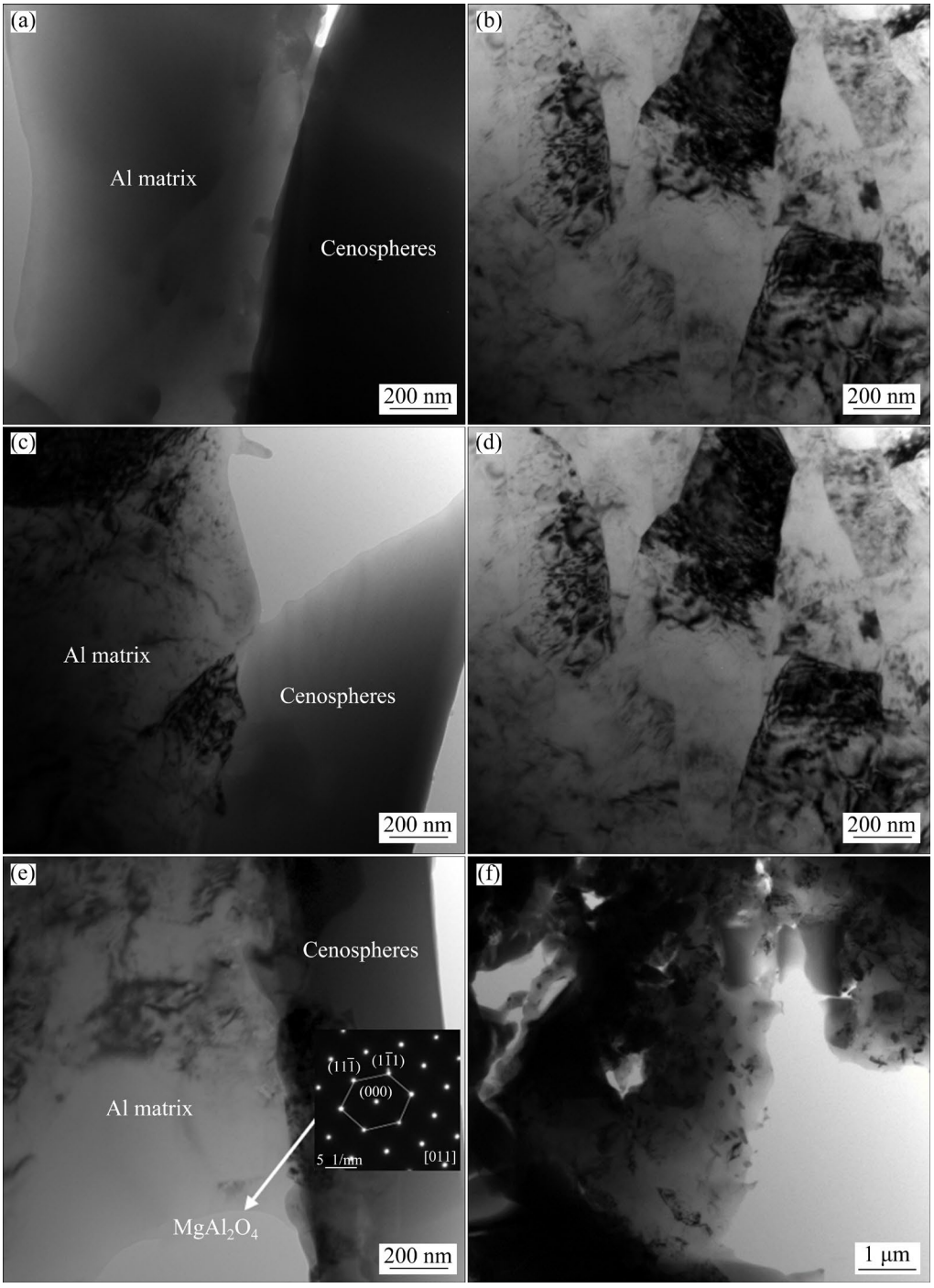

Fig. 3 TEM images of GCs/Al composites: (a, b) K46/1100Al; (c, d) K46/AA6061 in as-cast state; (e, f) K46/AA6061 after heat treatment

AA6061 is shown in Fig. 3(c), exhibiting a comparatively smooth microstructure devoid of interfacial reactant generation. There were numerous dislocations and subcrystalline boundaries that were entangled with each other, as displayed in Fig. 3(d). The subcrystalline boundary structure also contained a large number of dislocations. A great amount of dislocation entanglements and subcrystalline boundaries were generated by the significant thermal mismatch stress between Al and GCs caused by pressure infiltration. The microstructures of the heat-treated GCs/AA6061 composites are depicted in Figs. 3(e, f). The whole surface of the GCs was covered by the interfacial reaction products. Mg of AA6061 reacted with Al_2O_3 of GCs to produce the interfacial products,

which were identified as $MgAl_2O_4$ by diffraction spot calibration.

Furthermore, Mg was consumed in this reaction, which had a detrimental effect on the production of Mg_2Si following heat treatment. Due to the low content of Al_2O_3 in GCs, a considerable quantity of Mg_2Si was produced in the matrix. The phases produced in the matrix were uniformly distributed, as shown in Fig. 3(e). The increase in compressive strength of composite materials after heat treatment was mainly attributed to the formation of dispersive phases, as shown in Reaction (1):

$$4Al_2O_3+3Mg=3MgAl_2O_4+2Al \quad (1)$$

3.2 Damping performance of GCs/1100Al composites

The damping capacity (tan Φ)−strain curves of GCs/1100Al composites are displayed in Fig. 4. The damping capacity was reduced at low strains. When the strain increased, the damping value of K46/1100Al increased more obviously than that of S38/1100Al. When the strain was 0.3, the damping value of K46/1100Al reached 0.13, whereas that of S38/1100Al was only 0.09. According to research on the damping mechanism of metal materials, dislocation damping and interface damping constitute the majority of the damping mechanism [22]. Under mild strain, it is challenging to alter the interfacial strength when the strain varies. Therefore, the damping mechanism of GCs/1100Al is mainly dislocation damping when strain increases. According to Granato's dislocation vibration pinning model, the reciprocating motion of dislocations between pinning points generates damping. The dislocations reciprocated at the strong and weak pinning points to release the mechanical energy under strain. The area swept by the dislocation motion increased only in the reciprocating motion under the strong pinning effect of the pinning point, improving the damping value of the material. K46/1100Al had fewer solid pinning points or a longer distance between the strong pinning points than S38/1100Al, resulting in differences in their performance. As a result, K46/1100Al possessed a higher internal friction value than S38/1100Al under high strain conditions, which was in accordance with the damping mechanism of metal materials.

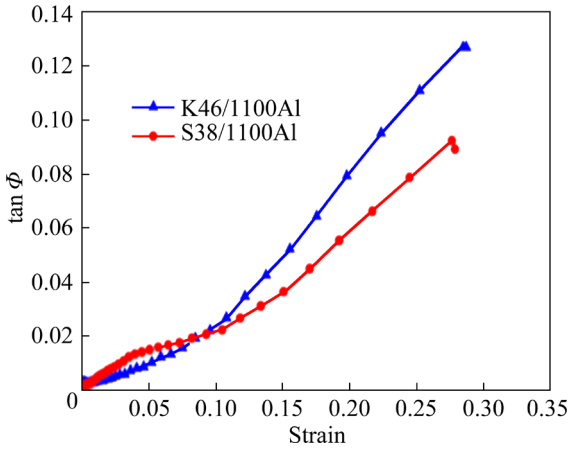

Fig. 4 Damping capacity−strain curves of different GCs/1100Al composites

The high-temperature damping mechanism of Al matrix composite primarily depends on the interfacial bond between the matrix and the reinforcement [14,17,18]. In this study, the volume fraction of GCs in the composites is approximately 60%, with numerous interfaces between the Al matrix and GCs. Therefore, we mainly discussed the impact of interfacial damping on GCs/1100Al composites. The damping capacity−temperature curves of GCs/1100Al composite at various frequencies are shown in Fig. 5. The damping performance trends of S38 and K46 composite materials were the same. With the increase of temperature, the damping value of the composites is approximately 0.03 and relatively stable below 300 °C. In the temperature range of 300−400 °C, the damping value increased dramatically from 0.03 to 0.08, which can be explained by the contact damping mechanism of the matrix. The interface of composites was well bonded in the temperature range of 25−300 °C, and the GCs and the matrix moved in tandem with the alternating load. At this time, the damping of the composites is mainly caused by the reciprocating motion of the dislocation at the pinning point. The mechanical value of the matrix decreased as the temperature rose, and the interfacial connection with cenospheres diminished. The hysteresis phenomenon dominated the increase in the damping value of GCs/1100Al at 300−400 °C, which led to strain hysteresis, stress generation, and some energy depletion.

Figure 5 shows the damping capacity changing trend with temperature in a specific way at different frequencies. When the frequency rose, the damping

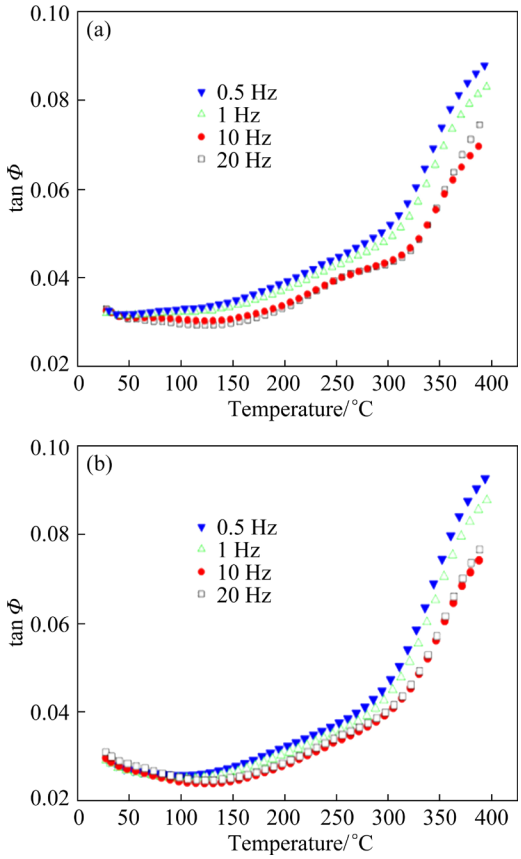

Fig. 5 Damping capacity−temperature curves of GCs/1100Al at different frequencies: (a) S38/1100Al; (b) K46/1100Al

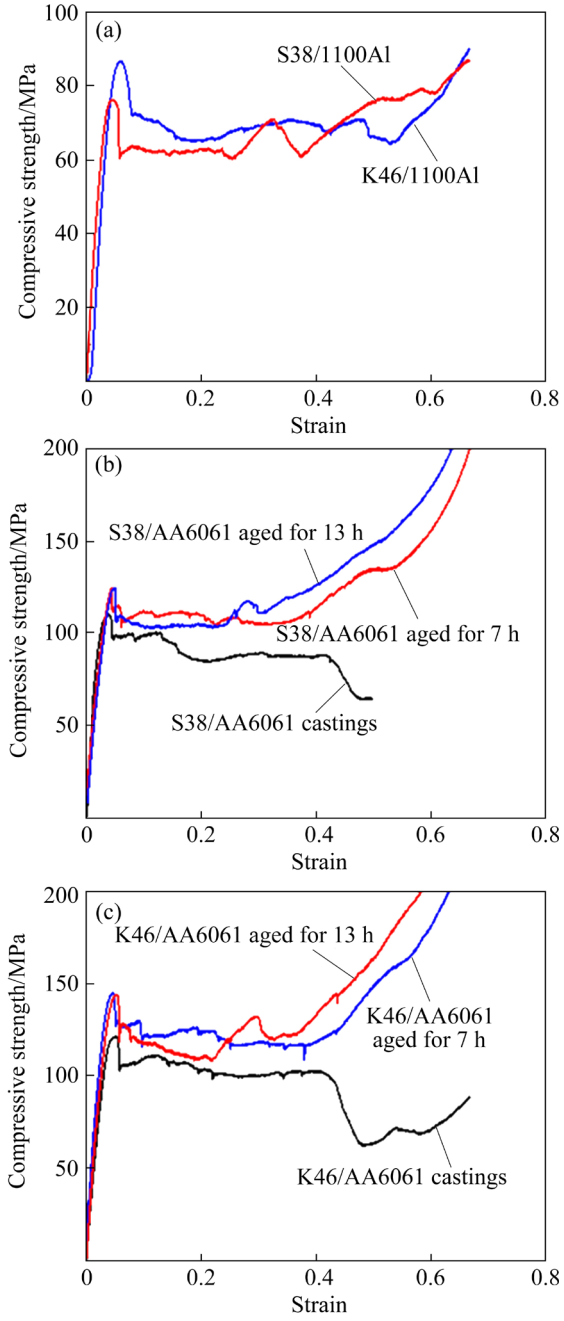

Fig. 6 Quasi-static compressive properties of Al matrix composites: (a) S38/1100Al and K46/1100Al; (b) S38/AA6061 castings and S38/AA6061 aged for 7 and 13 h; (c) K46/AA6061 castings and K46/AA6061 aged for 7 and 13 h

capability decreased. At 0.5 Hz, the damping capacity reached its maximum. The difference was determined by the properties of the material itself. It is known that the damping mechanism of temperature is the interface damping mechanism. Internal energy friction and hysteresis occur when the strain lags behind the stress. When the frequency is too high, the interface strain is unable to adapt to the frequency change at all, resulting in a low damping value of the material. When the frequency falls within a suitable range, the interface motion of the material may not be able to keep up with the frequency shift entirely. The substance exhibits a specific damping value.

3.3 Damping performance of GCs/AA6061 composites

GCs/AA6061 composites underwent heat treatment to increase their compressive strength, making them more suitable for application than GCs/1100Al composites (Fig. 6). The damping capacity−strain curves of the GCs/AA6061 composites aged for 7 and 13 h are shown in Fig. 7. As the strain increased, the damping value of S38/AA6061 rose. The damping values of the three states were comparable at low strains. After heat treatment, the damping value rose with increasing strain but only reached a value of approximately 0.06 at high strains, which was far less than the damping value of 0.13 for casting circumstances (Fig. 7(a)).

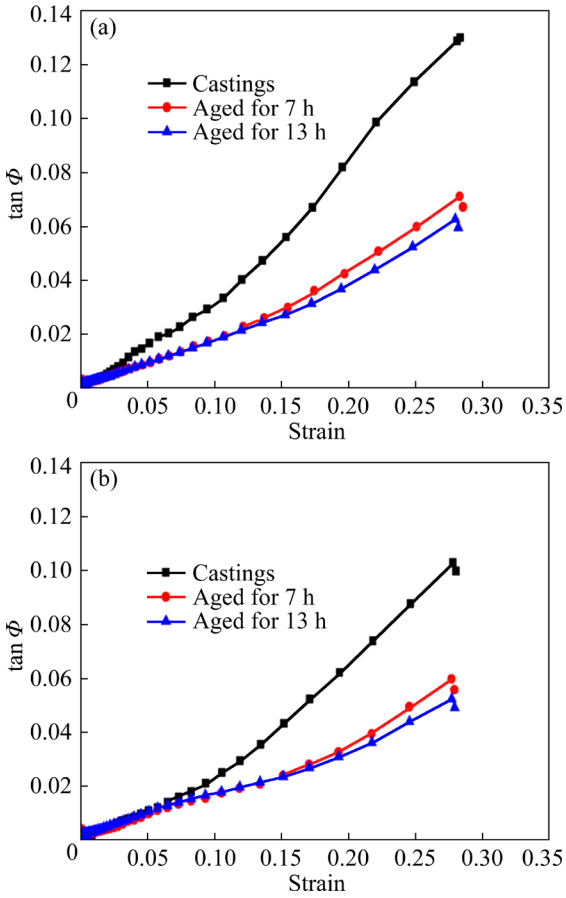

Fig. 7 Damping capacity−strain curves of GCs/AA6061 composites: (a) S38/AA6061; (b) K46/AA6061

According to the analysis of the dislocation damping mechanism, the changes in the number of solid pinning sites and the spacing between strong pinning points were caused by the change in the heat treatment state. Both the weak pinning point and the pinning point reciprocated the pinning action. When the strain was low, the density of pinning points was the same, the area swept by dislocation motion was uniform, and the damping value of the material was mostly not affected by the heat treatment state. However, as the strain increased, the weak pinning position of the casting material became unpinned, the area swept by the reciprocating motion of dislocations expanded, and the damping value of the material increased. The same phenomenon occurred in the heat-treated state. The area swept by dislocations was small, and the damping value decreased, which was due to the precipitation of second-order strong pinning points in composite materials, leading to a higher density of solid pinning points than the casting condition. Both (570 °C, 1 h) + (160 °C, 13 h) and (570 °C, 1 h) + (160 °C, 7 h) heat treatment processes were in their peak aging states, and the difference in the damping value was very small, roughly 0.01. Figure 7(b) displays the damping capacity−strain curves of K46/AA6061. The changing trend of damping value with strain for K46/AA6061 was identical to that of S38/AA6061.

The damping capacity−temperature curves of GCs/AA6061 composites at various frequencies are displayed in Fig. 8. The relationship between the damping value of S38/AA6061 and temperature in the casting state is depicted in Fig. 8(a), including three sections. Within the first range of 25−150 °C, the slope of the curve approached zero, and the damping value essentially remained basically unchanged. As the temperature rose to 150−300 °C, the damping value increased. The slope of the curve was not considerable, and the upward tendency was somewhat sluggish.

The interface damping mechanism was contributed to decreasing the interfacial bonding strength between the cenospheres and the matrix alloy as the temperature rose, causing the strain at the interface to lag behind the tension caused by the alternating load. Moreover, the external mechanical energy was consumed to overcome internal friction, which was then transformed into thermal energy. From 300 to 400 °C, the slopes of the curves in Fig. 8 quickly changed, and the overall damping value fluctuated dramatically. The interface damping and single dislocation damping were no longer mutually coupled. The interfacial bonding ability decreased with the increase of temperature, which occurred under alternating loads, converting mechanical energy consumption into thermal energy. The number of pinning points decreased as a result of some low-temperature inclusions in the casting material remelting at higher temperatures. The dislocation damping mechanism and the interface damping mechanism cooperated to produce a rapid increase in the damping value between 300 and 400 °C as the region swept by the reciprocating motion of dislocations increases. Furthermore, the frequency-dependent damping capacity changing trend of the S38/AA6061 was comparable to that of the S38/1100Al, which decreased as the frequency increased. This suggested that the relationship between damping value and frequency was independent of the matrix alloy composition of composites.

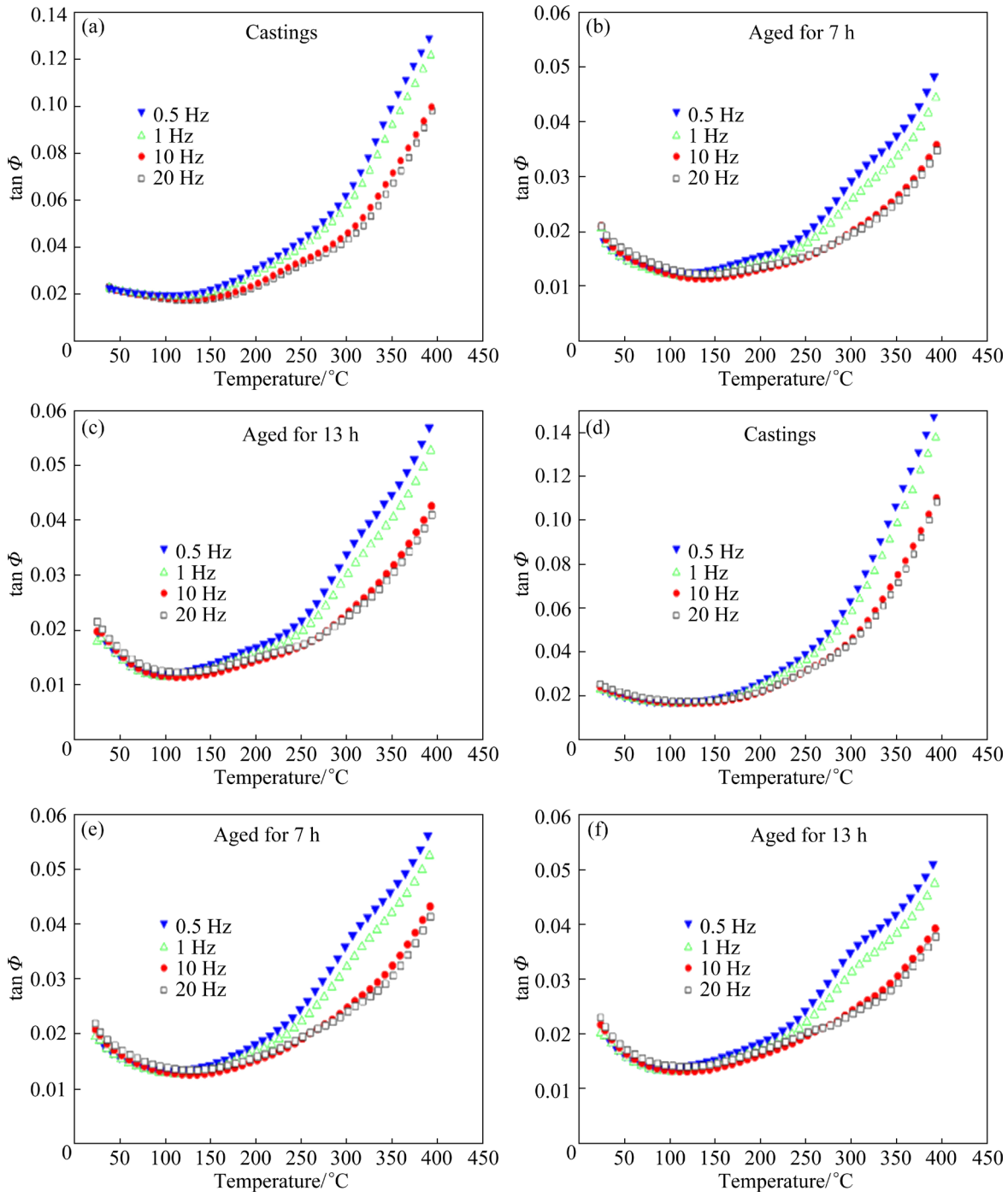

Fig. 8 Damping capacity−temperature curves of GCs/AA6061 at different frequencies: (a−c) S38/AA6061; (d−f) K46/AA6061

The damping capacity−temperature curves of S38/AA6061 at various frequencies following heat treatment are displayed in Figs. 8(b, c). There were two distinct stages in the damping capacity−temperature curves. The first phase occurred between 25 and 250 °C, with a damping value of approximately 0.01. The value remained constant despite different temperatures. Within the second temperature range of 250−400 °C, the damping value increased. The bonding strength of the matrix−reinforcement interface weakened at this point due to the high temperature. However, the second phase was generated during heat treatment, and its growth trend was much smaller than that of the casting condition. The strong pinning sites were these scattered phases that did not remelt as the

temperature rose. As things stand, the damping mechanism was solely dependent on the interface damping effect.

Figures 8(d−f) display the damping capacity−temperature curves of the K46/AA6061 composites. The damping capacity−temperature curve of K46/AA6061 exhibited a similar shifting tendency to that of S38/AA6061 before and after heat treatment. There was a three-stage changing trend in the capacity−temperature curve. The increasing trend of the damping capacity−temperature curve and the damping values at 25−150 °C and 150−300 °C were comparable to those of S38/AA6061. When the temperature rose, the damping values of K46/AA6061 were significantly different from those of S38/AA6061 at various frequencies in the temperature range of 300−400 °C. The damping value of K46/AA6061 was the same as that of S38/AA6061 at high frequencies of 10 and 20 Hz, increasing from 0.05 to approximately 0.10. Compared to S38/AA6061, the damping value of K46/AA6061 increased from 0.06 to 0.15 at 0.5 and 1 Hz, showing a more notable growth trend, which suggested that the wall thickness of the cenospheres influenced the damping value of the composites. It is well known that interface damping mostly contributes to the damping capacity−temperature curve of composites. The interface bonding strength between the matrix and the reinforcing phase had a major effect on the damping value of the composites as the temperature rose. The interface bonding strength of foam materials decreased with increasing temperature, and this drop was more noticeable in cenospheres with larger wall thicknesses than in the casting stage. The composites overcame the internal friction at the interface during alternating load, resulting in a high overall damping value and increased energy consumption.

Following heat treatment, the damping capacity−temperature curves of the K46/AA6061 composites are displayed in Figs. 8(e, f). After heat treatment, the damping capacity−temperature curves of K46/AA6061 at various frequencies and temperatures resembled those of S38/AA6061. However, the damping temperature of K46/AA6061 was higher than that of S38/AA6061 at low frequencies in the casting condition, which suggested that heat treatment stabilized the interfacial bonding in composites.

3.4 Damping mechanism of GCs/Al composites

The concepts of energy storage modulus and loss modulus in polymer materials were discussed in this research to examine the influence mechanism of storage modulus and loss modulus and assess the damping mechanism of GCs/Al composites.

3.4.1 Influence of matrix alloy on damping mechanism of composites

Figure 9(a) illustrates the impact of the matrix on the GCs/Al composites by displaying the trend of the S38/1100Al storage modulus and loss modulus as a function of strain. The loss modulus values of S38/AA6061 and S38/1100Al in the as-cast state followed the same pattern as the strain increased, with the same loss modulus value. The increasing trend of the S38/1100Al loss modulus was somewhat higher than that of S38/AA6061 as the strain rose. The storage modulus led to the strain-related discrepancy between S38/1100Al and S38/AA6061. S38/AA6061 had a much greater storage modulus than S38/1100Al, suggesting that the matrix alloy played a significant role in determining the energy storage modulus of composite materials. The energy storage modulus of AA6061 was greater than that of 1100Al, and the produced composite material had a larger storage modulus, which was consistent with earlier findings [12,23].

Furthermore, the storage modulus values of S38/1100Al and S38/AA6061 differed by approximately 3000 MPa under low and high strains. The modulus also dropped as the strain increased. The change in the storage modulus and loss modulus of K46/AA6061 with increasing strain is depicted in Fig. 9(b). The storage modulus of the matrix served as the primary factor responsible for the variation in the damping value produced utilizing two distinct matrix alloys. Although the loss modulus of various matrix alloys increased at the same rate, it did so in proportion to the increase in strain. Although the initial storage modulus of K46/AA6061 was noticeably larger than that of K46/1100Al, the energy modulus decreased at the same rate as the strain increased. Consequently, the variation in the storage modulus was the primary cause of the increased damping value of the composites made from 1100Al. The loss modulus rose and the storage modulus fell with increasing strain. The fluctuation between various matrix

alloys was constant, with the primary variation being the initial storage modulus value.

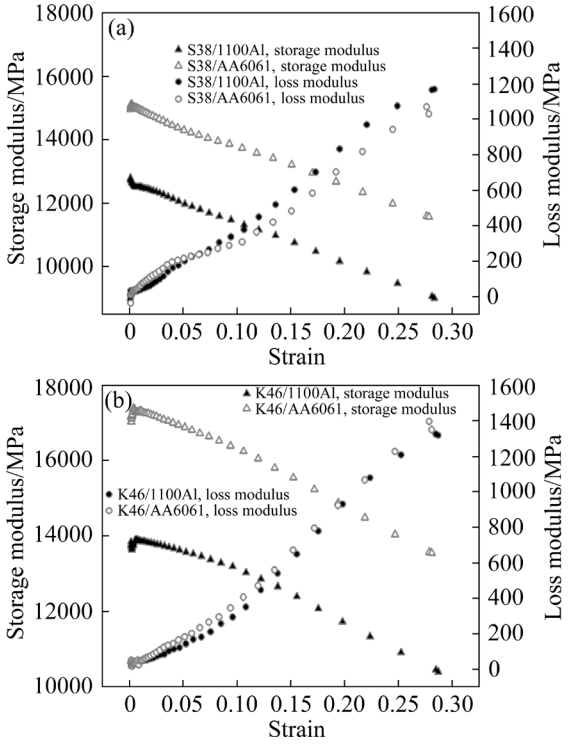

Fig. 9 Storage modulus−strain and loss modulus−strain curves with different matrixes and GCs: (a) S38/1100Al and S38/AA6061; (b) K46/1100Al and K46/AA6061

The storage modulus prepared with AA6061 possessed a higher starting value than that of 1100Al. According to the dislocation damping mechanism, the reciprocating motion of dislocations around the pinning point is the reason for damping syntactic composite materials. Dislocations during the reciprocating motion transformed mechanical energy into thermal energy, which resulted in the loss modulus. The two composites of the two matrix alloys had the same loss modulus, which suggested that the density of pinning points and the spacing between pinning points were comparable. Due to the comparability of the distance traveled and the area covered by the reciprocating motion of dislocations between the pinning locations, the changing trend of loss modulus was similar. Moreover, the reciprocating motion of the dislocation was independent of the storage modulus size, and it is a physical quantity based on the strength of the matrix alloy. Consequently, the larger the storage modulus is, the lower the damping value of the material under the same loss modulus.

3.4.2 Influence of GCs strength on damping mechanism of composites

The effect of GCs strength on the composite damping value was analyzed. K46/1100Al had a higher storage modulus than S38/1100Al, which was affected by the strength of the GCs, as shown in Fig. 9. The storage modulus of the prepared composite material increased with the increase of GCs compressive strength. In terms of the loss modulus, the modulus value of K46/1100Al became more significant than that of S38/1100Al as the strain increased. The difference between the two composites was only approximately 100 MPa. K46/AA6061 composites had a greater storage modulus than S38/AA6061, and their trend was similar to that of GCs/1100Al composites. On the other hand, the loss modulus increased monotonically as the strain increased, which corresponded to the growth pattern of the loss modulus of the GCs/1100Al composites. The difference in loss modulus was greater than that of GCs/1100Al under high strains, being approximately 300 MPa.

Dislocation damping is the primary mechanism responsible for the damping strain in the composites. Higher damping values and larger loss modulus are associated with wider areas swept by the reciprocating motion of the dislocation under the action of the pinning point. The density of pinning points in the 1100Al matrix was not significantly affected by the strength of the GCs, and the difference in the loss modulus for the GCsS/1100Al was not statistically significant. The areas of the composites prepared by the two cenospheres swept by the reciprocating motion of dislocations were the same.

The difference in the storage modulus of the GCs/AA6061 composites is mainly caused by the compressive strength of the GCs and the difference is basically the same with GCs/1100Al. K46/AA6061 possessed a larger loss modulus than S38/AA6061 when the strain increased. The depinning action of the weak pinning sites caused the dislocations in the composites to oscillate between the strong pinning points. The composites exhibited a higher loss modulus and a larger area swept by the dislocation action. K46/AA6061 had a lower density of solid pinning points than S38/AA6061. The formation of solid pinning points in the composites was specifically influenced by the strength of the GCs.

3.4.3 Effect of heat treatment on damping mechanism of GCs/AA6061 composites

The impact of heat treatment on the storage modulus and loss modulus of the GCs/AA6061 composites is depicted in Fig. 10. The changes in the storage modulus and loss modulus varied in different ways. The storage modulus and loss modulus change curves of S38/AA6061 with strain are shown in Fig. 10(a). After heat treatment, the storage modulus was different from that in the initial as-cast state. Additionally, the storage modulus of the aged material reached its maximum value after 13 h. After heat treatment, the original as-cast S38/AA6061 had a higher loss modulus than composites under all strain values.

The correlation between the storage modulus and loss modulus of K46/AA6061 in as-cast state and during heat treatment is depicted in Fig. 10(b). The storage modulus remained relatively constant. The initial value of energy storage modulus of K46/AA60601 was greater than that of S38/AA6061, and its decay trend with strain variation was less as well. The growth trend of the K46/AA6061 loss modulus underwent significant changes both in as-cast state and during heat treatment. They all exhibited a monotonically increasing growth pattern as the strain increased, although the growth rates varied. Under heat treatment circumstances, the loss modulus values of K46/AA6061 composites were the same at the beginning strain. The loss modulus growth trend of the as-cast K46/AA6061 composites was significantly larger with increasing strain than that of composites after heat treatment.

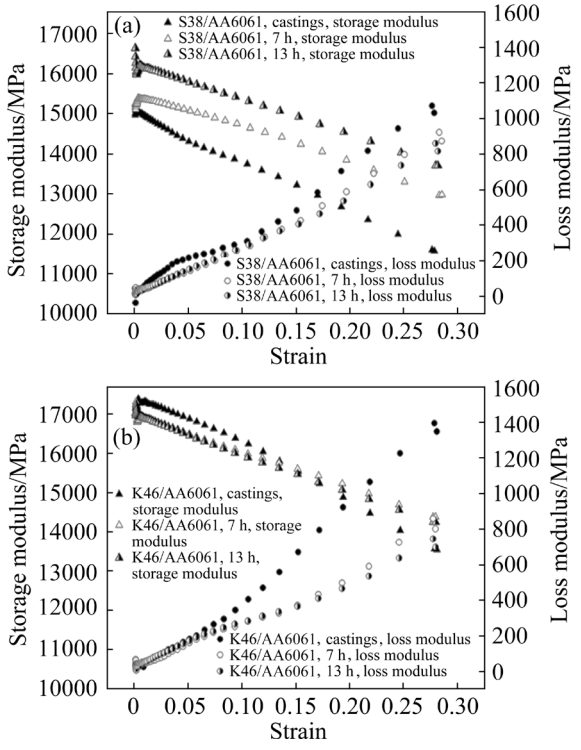

Fig. 10 Storage modulus−strain and loss modulus−strain curves of GCs/AA6061 composites in different heat treatment states: (a) S38/AA6061; (b) K46/AA6061

4 Conclusions

(1) Within the low frequency range from 0.5 to 20 Hz, the bonding strength between cenospheres and the aluminum matrix is notably high at lower temperatures (approximately room temperature to 100 °C). However, this strength diminishes as the temperature increases. The interfacial bonding strength of the composite materials between the reinforcement and the Al matrix decreased with increasing temperature. The damping capacity−temperature curve of composites was mainly caused by interface damping.

(2) The damping strain spectrum of the composites was investigated at low frequencies, specifically between 0.5 and 20 Hz. The presence of both strong and weak pinning points induced a reciprocating dislocation under low strain conditions, resulting in damping. The damping value increased as the strain grew.

(3) Following heat treatment, there was a considerable shift in the damping capacity−temperature curves of the GCs/AA6061 composites. The damping value increased as the strain and temperature rose, which demonstrated that heat treatment improved the material density of solid pinning sites and the interface bonding between the aluminum alloy and cenospheres.

(4) The storage modulus and loss modulus revealed that the variation in composite damping value was primarily caused by the initial storage modulus. After heat treatment, the loss modulus rose, and the storage modulus fell.

CRediT authorship contribution statement

Kai SUN: Investigation, Writing − Original draft; **Lin WANG:** Investigation, Visualization; **Hang SU:** Conceptualization, Methodology; **Jia-yi GENG:** Investigation, Software; **Qiang ZHANG:** Conceptualization, Methodology, Funding acquisition; **Bo MENG:** Methodology; **Zeng-yan WEI:** Writing − Review & editing; **Gao-hui WU:** Conceptualization, Supervision.

Declaration of competing interest

The authors declare that they have no known competing financial interests or personal relationships that could have appeared to influence the work reported in this paper.

Acknowledgements

This work was financially supported by the National Key Research and Development Program of China (No. 2022YFE0121400), the National Natural Science Foundation of China (Nos. 52071117, 52111530297, 51601047), the Heilongjiang Provincial Science Fund for Distinguished Young Scholars, China (No. JQ2021E002), and the Guangdong Basic and Applied Basic Research Foundation, China (No. 2022B1515120016).

References

[1] HUANG Wen-sen, CHEN Jia-hua, YAN Hong-ge, LI Qiang, XIA Wei-jun, SU Bin, ZHU Wei-jun. Solid solution strengthening and damping capacity of Mg−Ga binary alloys [J]. Transactions of Nonferrous Metals Society of China, 2022, 32: 2852−2865. https://doi.org/10.1016/S1003-6326(22)65988-0.

[2] LIU Jiao, LI Guo-xi, ZHU Ben-feng, DU Xiao-qing, YANG Yu-meng, WEI Guo-ying, ZHANG Zhao. Electrochemical noise energy generated by nickel electroplating process [J]. Transactions of Nonferrous Metals Society of China, 2023, 33: 951−957. https://doi.org/10.1016/S1003-6326(23)66158-8.

[3] JIANG H J, LIU C Y, MA Z Y, ZHANG X, YU L, MA M Z, LIU R P. Fabrication of Al−35Zn alloys with excellent damping capacity and mechanical properties [J]. Journal of Alloys and Compounds, 2017, 722: 138−144. https://doi.org/10.1016/j.jallcom.2017.06.091.

[4] LAI Tao, XU Ji-lin, XIAO Qi-fei, TONG Yun-xiang, HUANG Jun, ZHANG Jian-ping, LUO Jun-ming, LIU Yong. Preparation and characterization of porous NiTi alloys synthesized by microwave sintering using Mg space holder [J]. Transactions of Nonferrous Metals Society of China, 2021, 31: 485−498. https://doi.org/10.1016/S1003-6326(21)65511-5.

[5] PAN S A, DAI Q Y, SAFAEI B, QIN Z Y, CHU F L. Damping characteristics of carbon nanotube reinforced epoxy nanocomposite beams [J]. Thin-Walled Structures, 2021, 166: 108−127. https://doi.org/10.1016/j.tws.2021.108127.

[6] QIU Xue-jing, TANG Jia, TAN Jun, HU Hui-ping, JI Xiao-bo, HU Jiu-gang. Selective recovery of Cu(II) through polymer inclusion membranes mediated with 2-amino-methylpyridine derivatives [J]. Transactions of Nonferrous Metals Society of China, 2021, 31: 3591−3601. https://doi.org/10.1016/S1003-6326(21)65750-3.

[7] ZHAO J, JIANG N, ZHANG D S, HE B B, CHEN X. Study on optimization of damping performance and damping temperature range of silicone rubber by polyborosiloxane gel [J]. Polymers, 2020, 12: 1196. https://doi.org/10.3390/polym12051196.

[8] LEE S J, SHIN S E, USHIODA K, FUJII H. Microstructure, mechanical properties, and damping capacity in stir zone after friction stir welding of Fe−17Mn damping alloy [J]. Journal of Alloys and Compounds, 2019, 803: 1155−1167. https://doi.org/10.1016/j.jallcom.2019.06.367.

[9] CHEN Q, ZHANG H L, ZHOU S Q, CAI Y T, LI X G, XU Y. A novel high-entropy alloy with excellent damping property toward a large strain amplitude environment [J]. Journal of Alloys and Compounds, 2019, 802: 493−501. https://doi.org/10.1016/j. jallcom.2019.06.247.

[10] LI Z Z, LI X Y, YAN H G, CHEN J H, XIA W J, LI Q, SU B, SONG M. Achieving high damping and excellent ductility of AlMg alloy sheet by the coupling effect of Mg content and fine grain structure [J]. Materials Characterization, 2021, 174: 110974. https://doi.org/10.1016/j.matchar.2021.110974.

[11] WU G H, DOU Z Y, JIANG L T, CAO J H. Damping properties of aluminum matrix–fly ash composites [J]. Materials Letters, 2006, 60: 2945−2948. https://doi.org/10.1016/j.matlet.2006.02.018.

[12] KARE D, CHINTADA S, DORA S P. Damping behavior of Al/SiC composites fabricated by powder metallurgy [J]. Silicon, 2022, 14: 8255−8261. https://doi.org/10.1007/s12633-021-01497-3.

[13] PRASAD D S, SHOBA C. Experimental evaluation onto the damping behavior of Al/SiC/RHA hybrid composites [J]. Journal of Materials Research and Technology, 2016, 5: 123−130. https://doi.org/10.1016/j.jmrt.2015.08.001.

[14] WU J, LI C G, WANG D B, GUI M C. Damping and sound absorption properties of particle reinforced Al matrix composite foams [J]. Composites Science and Technology, 2003, 63: 569−574. https:// doi.org/10.1016/S0266-3538(02)00215-4.

[15] GUI M C, WANG D B, WU J J, YUAN G J, LI C G. Deformation and damping behaviors of foamed Al−Si−SiC_p composite [J]. Materials Science and Engineering: A, 2000, 286: 282−288. https://doi.org/10.1016/S0921-5093(00)00789-9.

[16] YANG K M, YANG X D, HE C N, LIU E Z, SHI C, MA L, LI Q, LI J, ZHAO N. Damping characteristics of Al matrix composite foams reinforced by in-situ grown carbon nanotubes [J]. Materials Letters, 2017, 209: 68−70. https://doi.org/10.1016/j. matlet.2017.07.126.

[17] BANHART J, BAUMEISTER J, WEBER M. Damping properties of aluminium foams [J]. Materials Science and Engineering: A, 1996, 205: 221−228. https://doi.org/10.1016/0921-5093(95)09973-5.

[18] SUN Kai, WANG Ling, ZHANG Qiang, MENG Bo, WEI Zeng-yan, SU Hang, WEI Guo-liang, GENG Jia-yi, WU Gao-hui. Boosting energy absorption performance of aluminum matrix syntactic foam with carbon coated glass cenospheres [J]. Composites Communications, 2023, 43: 101718. https://doi.org/10.1016/j.coco.2023.101718.

[19] MU Y, YAO G, ZU G, CAO Z. Influence of strain amplitude on damping property of aluminum foams reinforced with copper-coated carbon fibers [J]. Materials & Design, 2010, 31: 4423−4426. https://doi.org/10.1016/j.matdes.2010.04.025.

[20] SUN Kai, WANG Ling, ZHANG Qiang, MENG Bo, WEI Zeng-yan, SU Hang, WEI Guo-liang, SHIL'KO S V, WU Gao-hui. Preparation and quasi-static compression properties of hybrid aluminum matrix syntactic foam reinforced with GCs and silicon carbide nanowires [J]. Materials Characterization, 2023, 195: 112496. https://doi.org/10.1016/j.matchar.2022.112496.

[21] DONG R, YANG W, YU Z, WU P, HUSSAIN M, JIANG L, WU G. Aging behavior of AA6061 matrix composite reinforced with high content SiC nanowires [J]. Journal of Alloys and Compounds 2015, 649: 1037−1042. https://doi.org/10.1016/j.jallcom.2015.07.233.

[22] GRANATO A, LÜCKE K. Theory of mechanical damping due to dislocations [J]. Journal of applied physics 1956, 27: 583−593. https://doi.org/10.1063/1.1722436.

[23] REDDY K V, NAIK R B, RAO G R, REDDY G M, KUMAR R A. Microstructure and damping capacity of AA6061/graphite surface composites produced through friction stir processing [J]. Composites Communications, 2020, 20: 100352. https://doi.org/10.1016/j.coco.2020.04.018.

玻璃空心微珠增强铝基多孔复合材料的阻尼性能和机理

孙 凯[1]，王 琳[1]，苏 航[2]，耿家一[1]，张 强[1]，孟 波[3]，卫增岩[1]，武高辉[1]

1. 哈尔滨工业大学 材料科学与工程学院，哈尔滨 150001；
2. 石油管材及装备材料性能与结构安全国家重点实验室，西安 710000；
3. 山东省建筑科学研究院有限公司 山东省建筑工程质量检验测试中心，济南 250031

摘 要：通过压力浸渗法制备玻璃空心微珠增强铝基复合材料，从而改善其阻尼特性。采用透射电子显微镜和扫描电子显微镜对复合材料的显微组织进行表征。使用动态机械热分析仪测定低频阻尼特性，旨在探讨阻尼能力随应变、温度和频率变化的趋势。研究结果表明，阻尼值随着温度和应变的增加而增大，其最大值为 0.15。此外，当频率增加时，阻尼值降低。应变下的位错阻尼和温度下的界面阻尼是两种主要的阻尼机制。热处理后，位错强钉扎点密度的增加降低了阻尼值，这是因为热处理增强了复合材料的界面结合力。

关键词：玻璃空心微珠；铝基复合材料；显微组织；低频阻尼性能

(Edited by Wei-ping CHEN)